Heliyon

*Received:*
30 April 2018
*Revised:*
18 July 2018
*Accepted:*
12 November 2018

Cite as: Ayad Mutafi, N. Yidris, M. R. Ishak, R. Zahari. An investigation on longitudinal residual strains distribution of thin-walled press-braked cold formed steel sections using 3D FEM technique.
Heliyon 4 (2018) e00937.
doi: 10.1016/j.heliyon.2018.e00937

# An investigation on longitudinal residual strains distribution of thin-walled press-braked cold formed steel sections using 3D FEM technique

**Ayad Mutafi** [a,b], **N. Yidris** [a,*], **M. R. Ishak** [a], **R. Zahari** [a]

[a] *Department of Aerospace Engineering, Universiti Putra Malaysia, 43400, Serdang, Selangor, Malaysia*

[b] *Faculty of Engineering and Petroleum, Hadhramout University, Mukalla, Yemen*

[*] Corresponding author.

E-mail address: nyidris@upm.edu.my (N. Yidris).

## Abstract

Steel sections are normally shaped via cold work manufacturing processes. The extent of cold work to shape the steel sections might induce residual stresses in the region of bending. Previously, researchers had performed studies on the influences of local buckling on the failure behavior of steel compression members which shown that failure will happen when most of the yielding has extended to the middle surface in the bend region of the sections. Therefore, these cold work methods may have major effect on the behavior of the steel section and also its load-bearing capability. In addition, another factor may play significant role in formed section's load-bearing capacity which is the longitudinal residual strain. The longitudinal residual strain raised during forming procedure can be used to define the section imperfection of the formed section and its relation to the existence of defects. Therefore, the main motivation of this research paper is to perform three-dimensional finite element (3D-FE) to investigate peak longitudinal residual strains of a thin-walled steel plate with

https://doi.org/10.1016/j.heliyon.2018.e00937

large bending angle along member length. A 3D finite element simulation in ABAQUS has been employed to simulate this forming process. The study concluded that the longitudinal residual strain at the section corner edge was higher than those at the rest of the corner region. These strains at the edge were higher than the yield strain ($\boldsymbol{\varepsilon_y}$) of the formed section which occurred due to the lack of transverse restraint. This made the plate edge tended to bend toward the normal direction when it was under a high transverse bending. This causes a significant difference in longitudinal strain at the plate edge.

Keyword: Structural engineering

## 1. Introduction

Steel sections are typically shaped via cold work manufacturing processes. The extent of cold work to shape the steel sections might induce residual stresses in the region of bending. Loughlan et al [1] studied the influence of local buckling on thin-walled steel sections have presented that final failure will follow when most of the yielding has extended to the middle surface in the bend region of the sections. Therefore, these cold work practice may have major effect on the behavior of the steel section and also its load-bearing capability [2]. In addition, another factor may play significant role in formed section's load-bearing capacity is the longitudinal residual strain. The longitudinal residual strain raised during forming procedure can be used to define the section imperfection of the formed section and its relation to the existence of defects [3].

The longitudinal strain growth due to forming is essential in order to evaluate the severity of a forming process. Therefore, it is always highlighted in related studies. Farzin et al. [4] explained that the main cause of the longitudinal strain is because of their stretched longitudinal fibers in a flange during forming of sheet metal. After the longitudinal strain is larger than the elastic strain limit, plastic deformation takes place and if the stresses/strains reach to a point which they are unbalanced after unloading, then product defects are induced. Weng and Peköz [5] used electrical discharge machining (EDM) technique to measure residual strains to estimate residual stresses. Quach et al. [6] developed a closed formed analytical solution to determine residual stresses/strains raised from coiling-uncoiling process. Also, Quach et al. [7] implemented two-dimensional finite element modeling (2D-FEM) to measure residual stresses/strains as the alternative to laboratory measurements. Amouzegar et al. [8] developed a numerical algorithm to estimate the residual stresses and strains through-thickness variation of thin-walled sections. Gerbo et al. [9] introduced 3D digital image correlation (DIC) as a new nondestructive approach for measuring residual strains in press-braked thick steel plate with small bending angle ($\leq$30°). He performed 2D and 3D FEM to validate the new approach and


https://doi.org/10.1016/j.heliyon.2018.e00937

recommended 3D-FE for detailed investigation. Gerbo concluded that the residual strains at the plate edge were higher than those at the mid-plate zone. Quach et al. [2] expected a longitudinal variation of residual stresses/strains along the section length, but did not explain the reason of this distribution changes. In addition, M Abambres et al. [10] mentioned that this matter is neglected in the literature due to the lack of studies (Experimental and Numerical) for verification. Therefore, the main motivation of this research paper was to perform 3D-FE to investigate peak longitudinal residual strains of a thin-walled steel plate with large bending angle ($\approx 90^{\circ}$) along member length.

## 2. Methodology

### 2.1. Scope on press-braking operation

Press braking is one of the metal forming processes in which a flat sheet metal is positioned between a punch and die and bent along its length in order to form section corners as shown in Fig. 1. The finite element procedure is used to estimate the residual stresses due to the press-braking process. The corner region is expected to experience high stamping force as a result of the contact between the punch and the metal sheet. This work simulated a section tested by Weng and Peköz [5]. Their experimental results are important for the finite element results validation purposes. This study was performed for a single bend to investigate the longitudinal residual

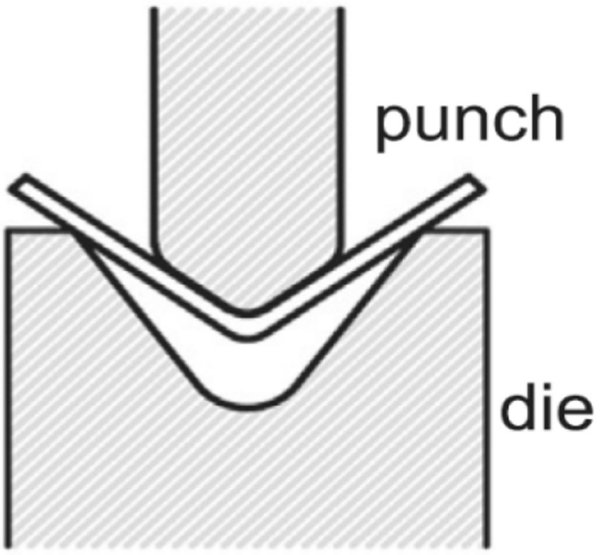


**Fig. 1.** Press-braking forming process of sheet metals, reproduced by permission from [8].


https://doi.org/10.1016/j.heliyon.2018.e00937

strain. Hence, the results presented in this section is for a single corner perimeter of PBC14 and P16 specimens.

## 2.2. FE model description

This study implemented an explicit finite element code in ABAQUS [11] to simulate the press-braking process which is effective in quasi-static problems such as metal forming. This study intended to form and investigate one corner of lipped channel section, as shown in Fig. 2. Therefore, the dimensions of the sheet were 50 × 100 mm (width × length) to investigate the longitudinal residual strain from the corner region due to the press-braking operation, as shown in Fig. 3. This study is a part of research intended to investigate the press-braking process influence on buckling and post-buckling of thin-walled cold formed steel sections. Therefore, the selection of 100 mm length is to the highest dimension in the section geometry for simulation according to Table 1. The model contains three parts: steel sheet, punch, and die. Punch and die modeling was performed via an analytical rigid model and the steel sheets were deformable shells were modeled first as a deformable solid with C3D8R element. The C3D8R element is an 8-node linear brick with reduced integration and hourglass control [11]. The general contact were the featured interaction between the model parts. The geometrical properties are presented in Table 1.

For boundary conditions the steel sheet was set to be free in three translational movements as well as its rotations. This simulation intended to implement displacement loading therefore Displacement was applied to the punch to allow it to move in the y-direction only in order to bend the steel sheet. For the die, it was restricted from moving by applying fixed boundary conditions at its reference point (RP).


**Fig. 2.** Dimensions of the lipped channel section.


https://doi.org/10.1016/j.heliyon.2018.e00937

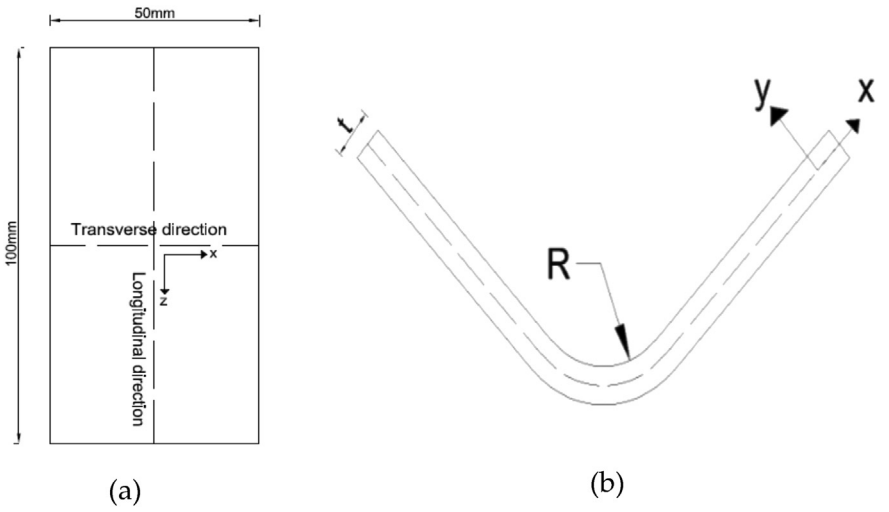


**Fig. 3.** Dimensions and coordinate system of the plate: (a) plan view before bending and (b) elevation view after bending(web-flange corner).

**Table 1.** Geomatrical and material properties of a lipped channel section.

| Specimen | t (mm) | a (mm) | b (mm) | c (mm) | R (mm) | $\sigma_y$ (MPa) | $\sigma_u$ (MPa) | $\varepsilon_y$ (x $10^{-6}$) | E (GPa) | n (x$10^{-2}$) | $\varepsilon_u{}^a$% |
|---|---|---|---|---|---|---|---|---|---|---|---|
| PBC 14 | 1.80 | 76.23 | 41.45 | 15.37 | 3.96 | 250.1 | 345.0 | 1230 | 203.3 | 9.56 | 33 |
| P16 | 1.63 | 67.18 | 34.98 | 15.82 | 2.39 | 220.9 | 310.7 | 1090 | 202.7 | 9.74 | 32 |

## 2.3. Material properties

Material non-linearity modeling in ABAQUS [11] uses true stress−logarithmic plastic strain data up to the final point. These data can be derived from the nominal stress−strain data using Eqs. (1) and (2). The curves related to the true stress−logarithmic plastic strain, true stress−strain, and nominal stress−strain are shown in Fig. 4. Weng and Peköz [5] have not provided the experimental stress−strain curves for specimens PBC14 and P16 [7]:

$$\sigma = E\varepsilon, \ \ \varepsilon \leq \sigma_y/E \tag{1}$$

$$\sigma = \sigma_y \left(\frac{E\varepsilon}{\sigma_y}\right)^n, \quad \varepsilon > \sigma_y/E \tag{2}$$

where R is radius of the corner, $\sigma_y$ is yield stress, $\sigma_u$ is ultimate stress, $\varepsilon_y$ is yield strain, E is modulus of elasticity, and $\varepsilon_u$ is ultimate strain.

## 2.4. Mesh convergence study

The studies of mesh independency is crucial in a numerical simulation to set the limit of the model mesh density. Transverse residual strain at inner/outer mid-corners


https://doi.org/10.1016/j.heliyon.2018.e00937

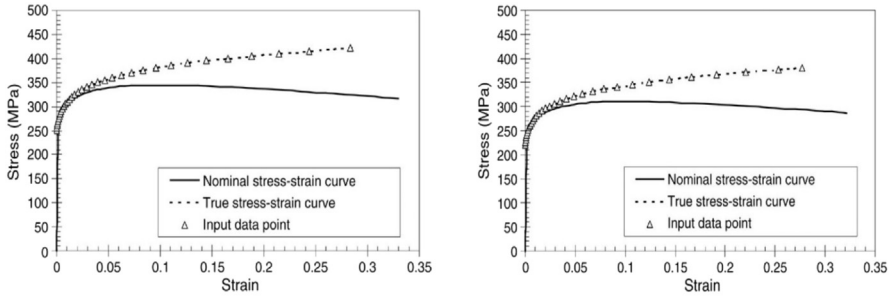


**Fig. 4.** Stress−strain curve: (a) PBC14 steel lipped channel, reproduced by permission from [7] and (b) P16 steel lipped channel, reproduced by permission from [7].

were monitored for four different meshes. The number of elements at the shorter edge were more than the longer edge, as at this location, the metal sheet interacts with the punch and die, hence a large bending occurred. Tables 2 and 3 show the outcomes of the convergence test.

From Tables 2 and 3, the extra fine mesh density was used as a reference to examine the accurateness of the other three mesh densities. It can be noticed that the medium mesh displayed outcomes closer to that of the finer mesh. Hence, the medium mesh density has been chosen for this study.

**Table 2.** Evaluation of maximum transverse strain for PBC14 at mid-corner.

| Mesh type | No. of elements | Max. transverse residual strain | | | |
|---|---|---|---|---|---|
| | | $\varepsilon_x$ (inner) | Diff. % | $\varepsilon_x$(outer) | Diff. % |
| Coarse | 160,000 | −0.247 | 2.0 | 0.250 | 4.5 |
| Medium (Adopted) | 240,000 | −0.251 | 0.4 | 0.260 | 0.8 |
| Fine | 360,000 | −0.251 | 0.4 | 0.266 | 1.5 |
| Extra Fine | 480,000 | −0.252 | 0.0 | 0.262 | 0.00 |

**Table 3.** Evaluation of maximum transverse strain for P16 at mid-corner.

| Mesh type | No. of elements | Max. transverse residual strain | | | |
|---|---|---|---|---|---|
| | | $\varepsilon_x$ (inner) | Diff. % | $\varepsilon_x$(outer) | Diff. % |
| Coarse | 160,000 | −0.345 | 9.8 | 0.332 | 5.7 |
| Medium (Adopted) | 240,000 | −0.382 | 0.8 | 0.352 | 0.3 |
| Fine | 360,000 | −0.376 | 0.8 | 0.348 | 0.9 |
| Extra Fine | 480,000 | −0.379 | 0.0 | 0.351 | 0.00 |


https://doi.org/10.1016/j.heliyon.2018.e00937

## 3. Results and discussion

### 3.1. Results validation

The finite element results compared with the simplified analytical predictions for transverse strains to validate it. Kervick and Springborn [12] presented a formula of maximum transverse strain with a consideration of assumptions: a homogeneous material, the neutral axis remains at the plate centreline, the plane sections remain plane, and the plate is subject to pure bending. A mechanics-based approach to predict the transverse residual strains ($\varepsilon_x$) is:

$$\varepsilon_x = \frac{-y}{R} \tag{3}$$

where y is the distance from center line to the surface. The negative sign indicates tensile and positive sign refers to compressive. However as noted by Cook [13], plastic bending operation cause the neutral axis shifts toward the compressive face of the plate by around 5%. By taking this assumption into account, the prediction for the transverse strain ($\varepsilon_x$) can be modified as follows:

$$\varepsilon_x = \frac{-y + 0.05t}{R + 0.45t} \tag{4}$$

Johnson and Mellor [14] also gave an empirical formulation that is relevant for bend angles exceeding 70° and for width to thickness ratios of more than 10. This formula considers the neutral axis shift by around 5% toward the compressive face. The equation is as follows:

$$\varepsilon_x = \frac{-y + 0.05t}{R + 0.55t} \tag{5}$$

This research considered these equations for validation. To ensure validation accuracy, three transverse line were selected (z = 0L, 0.5L, and 0.7L).

Fig. 5 shows the comparison of the transverse residual strain obtained from 3D-FE analysis and the predictions by Eqs. (3), (4), and (5). As the analytical predictions assume the peak transverse residual strain is linear along the corner region. In addition, the numerical results are able to estimate the strain at each point to the plate. Therefore, the comparison here is between the peak strains in the analytical predictions and those in the numerical results.

From Fig. 5a, the comparison between the 3D-FE results and the analytical predictions showed a close agreement for z = 0L, 0.5L, and 0.7L at 99%−67%. From Fig. 5b, the comparison showed close agreement at 97%−77%. For z = 0L, the residual strain was higher than that at the mid-plate zone.


https://doi.org/10.1016/j.heliyon.2018.e00937

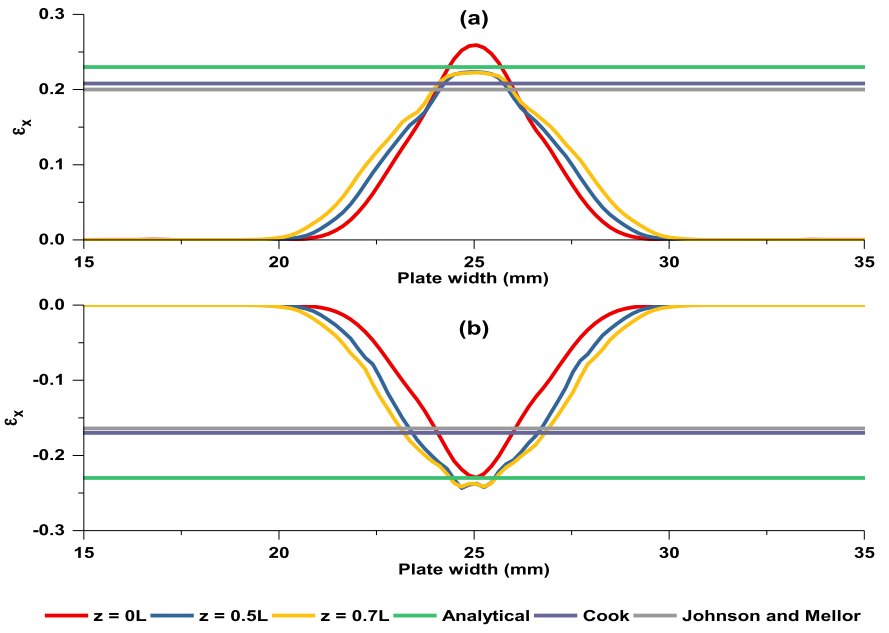


**Fig. 5.** Transverse residual strain comparison (specimen PBC14): (a) Inner surface, (b) Outer surface.

From Fig. 6a, the comparison between the 3D-FE results in specimen P16 and the analytical predictions showed a close agreements for z = 0L, 0.5L, and 0.7L at 92%−60%. However, for z = 0L, the peak strain was lower than those for z = 0.5L and 0.7L. From Fig. 6b, the comparison showed a close agreement for z = 0L, 0.5L, and 0.7L at 99%−78%.

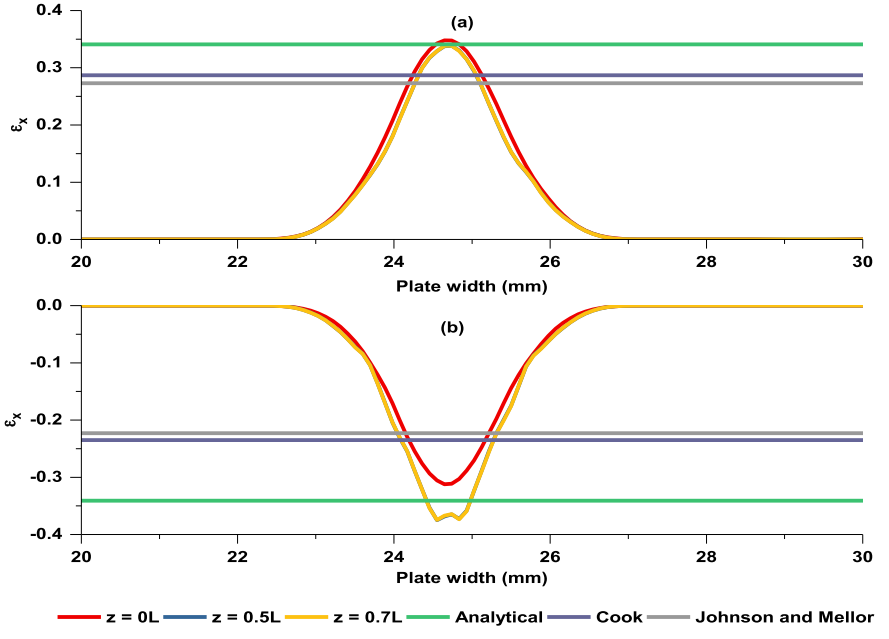


**Fig. 6.** Transverse residual strain comparison (specimen P16): (a) Inner surface, (b) Outer surface.


https://doi.org/10.1016/j.heliyon.2018.e00937

The 3D-FE was able to predict the residual strain and agreed with the analytical predications in the range. Therefore, the 3D-FE results are considered valid.

## 3.2. Longitudinal residual strain distribution

Fig. 7 shows the longitudinal residual strain ($\varepsilon_z$) distribution at the corner region of the formed section. The mid-corner at the edge indicates different strain state from the rest of the corner zone. At the inner surface, the compressive strain (positive strain) covers most of the corner zone although the strain starts to turn to tensile (negative strain) near the edge. Likewise, at the outer surface, the tensile strain (negative strain) covers most of the corner zone although the strain starts to turn to compressive (positive strain) near the edge.

In addition, the strain at the edges are higher than those at the rest of the corner zone. This can be explained that at the free edge, Poisson's effect induces stresses rather than strain in the longitudinal direction. In other words, the plate approaches plane stress state at the edge and plane strain at the rest of the corner zone.

The lack of transverse restraint at the plate edge plays a significant role in strain state especially the longitudinal strain. This lack of restraint (free edge), large bending angle, and plate width to thickness ratio cause the corner edge to soften and bow downward in the normal direction. Therefore, residual strain will develop and induce higher amount at the edge than those at the rest of the corner zone. Fig. 8 shows a longitudinal section view of the deformed plate. It shows the bend downward where at the free end strains are higher and start to decrease away from the free end.

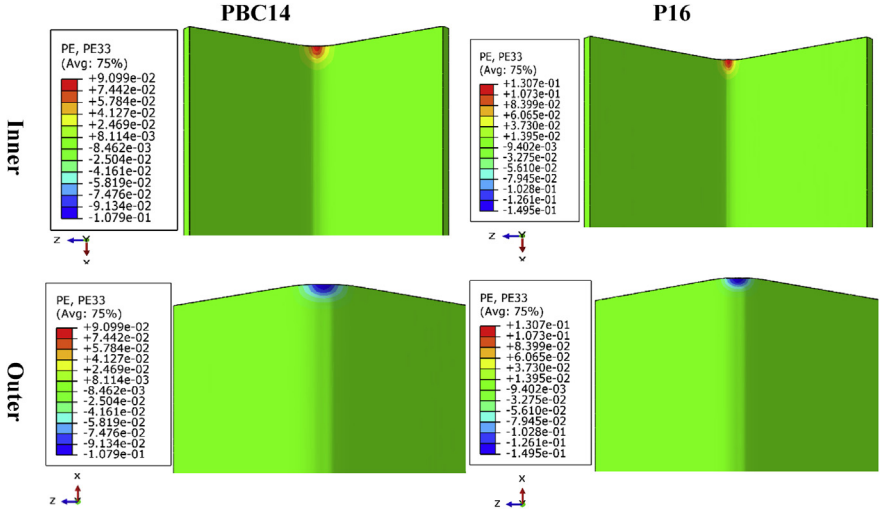


**Fig. 7.** Specimens deformed shape and longitudinal residual strain ($\varepsilon_z$).


https://doi.org/10.1016/j.heliyon.2018.e00937

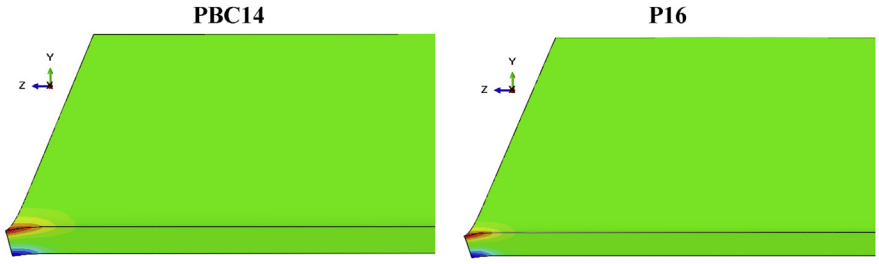


**Fig. 8.** Section view (longitudinal).

## 3.3. Peak longitudinal residual strain

Previous studies assumed that the peak longitudinal residual strain is linear along the corner length. These studies implemented experimental and numerical techniques to estimate the residual strain. However, preceding section shows that the longitudinal residual strain has a different state at the corner edge. Therefore, this section discusses the peak longitudinal residual strain estimated in this study and compares it with the experimental results estimated by Weng and Peköz [5] and 2D finite element estimated by Quach et al. [7].

### *3.3.1. Longitudinal residual strains before cold bending*

Weng and Peköz [5] found that the residual strain in the flat plate could be up to 40% of the yield strains. These strains existence is due to coiling and uncoiling processes. Quach et al. [7] used the analytical solution developed by Quach et al. [6] to initialize strains developed by coiling−uncoiling process for samples PBC14 and P16 measured by Weng [5]. Also, by trial and error, they determined the coil diameter to fit with the 2D-FE results (D = 1100 mm). Similarly, this study considered the same coil diameter as determined by Quach et al. In this study, the analytical solution provided by Quach et al. [6] for the residual strains developed from coil−uncoiling processes was considered. The determined longitudinal residual strains from the analytical solution was imposed to the finite element results to compare with the results from Weng and Quach et al. [5,7].

The total longitudinal strain of any point at the onset of reverse yielding during uncoiling is

$$\varepsilon_{z,uy} = \left(\kappa_c + \kappa_{uy}\right) y \tag{6}$$

The residual stresses and strains develop if coil curvature $k_c$ equals or exceeds the coil curvature limit $\kappa_{cy}$. Therefore by assuming:

$$\kappa_c = \kappa_{cy} \tag{7}$$


https://doi.org/10.1016/j.heliyon.2018.e00937

So,

$$\kappa_{cy} = \kappa_c = \frac{2\sigma_y(1-\nu^2)}{Et\sqrt{1-\nu+\nu^2}} \tag{8}$$

In general, during coiling, the central portion $|y|$ of the thickness experiences elastic bending with the longitudinal and transverse stresses due to a coiling curvature $k_c$. This $|y|$ is defined by:

$$|y| \leq y_{cy} = \frac{\sigma_y(1-\nu^2)}{E\kappa_c\sqrt{1-\nu+\nu^2}} \tag{9}$$

where $y_{cy}$ separates the elastic $|y|$ from the elastic−plastic outer portions. This leads to the uncoil curvature limit $k_{uy}$:

$$k_{uy} = -\frac{\sigma_y(1-\nu^2)[2-\nu+\omega_c(2\nu-1)]}{E|y|(1-\nu+\nu^2)\sqrt{1-\omega_c+\omega_c^2}} \tag{10}$$

where $\omega_c$ is the coil stress ratio which can be determined using:

$$|y| = \frac{\sigma_y(1-\nu^2)}{E\kappa_c\sqrt{1-\nu+\nu^2}} + \frac{\sigma_y}{E\kappa_c}\left[\frac{\omega_c(1-2\nu)}{\sqrt{1-\omega_c+\omega_c^2}} + \frac{\sqrt{3}}{2}coth^{-1}\left(\sqrt{\frac{4\left(1-\omega_c+\omega_c^2\right)}{3}}\right)\right]_{\nu}^{\omega_c} \tag{11}$$

So, the final longitudinal strain $\varepsilon_{z,r}$ can be determined from the following equation:- where $\omega_u$ is the uncoiling stress ratio and $\omega_{uy}$

$$\varepsilon_{z,r} - \varepsilon_{z,uy} = \mp\frac{\sigma_y}{E\kappa_c}\left[\frac{\omega_c(1-2\nu)}{\sqrt{1-\omega_c+\omega_c^2}} + \frac{\sqrt{3}}{2}coth^{-1}\left(\sqrt{\frac{4\left(1-\omega_c+\omega_c^2\right)}{3}}\right)\right]_{\omega_u y}^{\omega_u} \tag{12}$$

where $\omega_u$ is the uncoiling stress ratio and $\omega_{uy}$ is the corresponding stress ratio. Both can be obtained from:

$$\omega_u = \frac{\sigma_{x,c} + \sigma_{x,u}}{\sigma_{z,c} + \sigma_{z,u}} \tag{13}$$

where $\sigma_{x,c}$ and $\sigma_{x,u}$ are the transverse residual stresses from coiling and uncoiling processes, respectively, and $\sigma_{z,c}$ and $\sigma_{z,u}$ are the longitudinal residual stresses from coiling and uncoiling processes, respectively.

$$\omega_{uy} = \frac{[(1-\nu^2)\omega_c - \nu(2-\nu)]}{[(1-2\nu)\omega_c - (1-\nu^2)]} \tag{14}$$


https://doi.org/10.1016/j.heliyon.2018.e00937

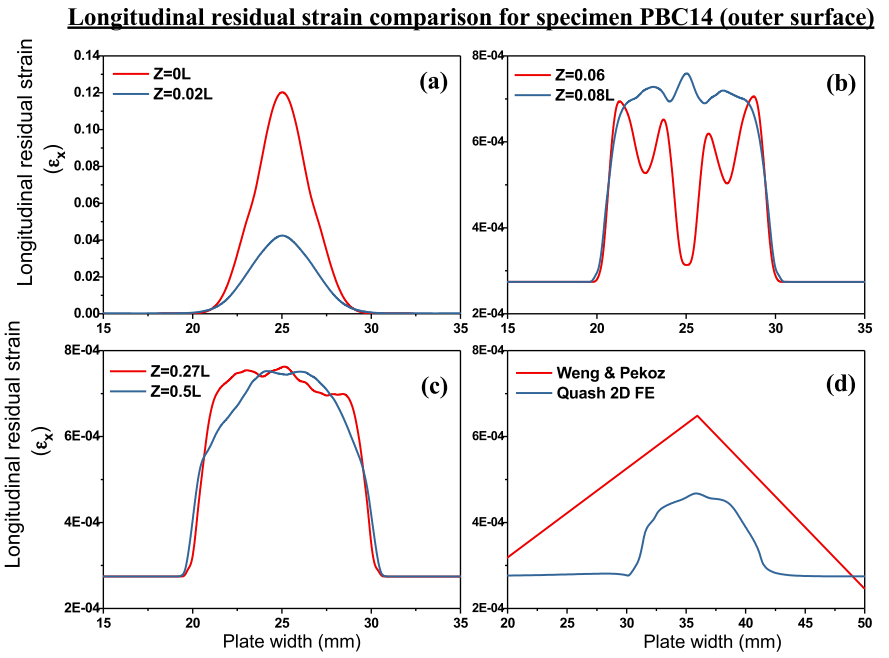


**Fig. 9.** Longitudinal residual strain comparison for specimen PBC14 (outer surface): (a) 3D-FE (0L and 0.02L), (b) 3D-FE (0.06L and 0.08L), (c) 3D-FE (0.27L and 0.5L), and (d) 2D-FE, Experiment.

Therefore, analytical solution -Eqs. (6), (7), (8), (9), (10), (11), (12), (13), and (14) - helps to determine longitudinal residual strain due to coiling-uncoiling process to be presented in the next section.

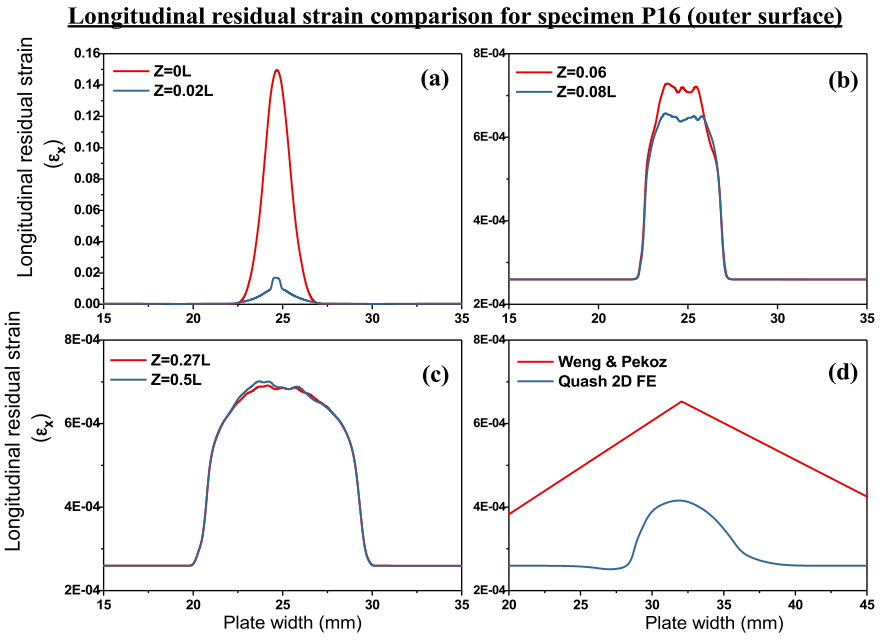


**Fig. 10.** Longitudinal residual strain comparison for specimen P16 (outer surface): (a) 3D-FE (0L and 0.02L), (b) 3D-FE (0.06L and 0.08L), (c) 3D-FE (0.27L and 0.5L), and (d) 2D-FE, Experiment.


https://doi.org/10.1016/j.heliyon.2018.e00937

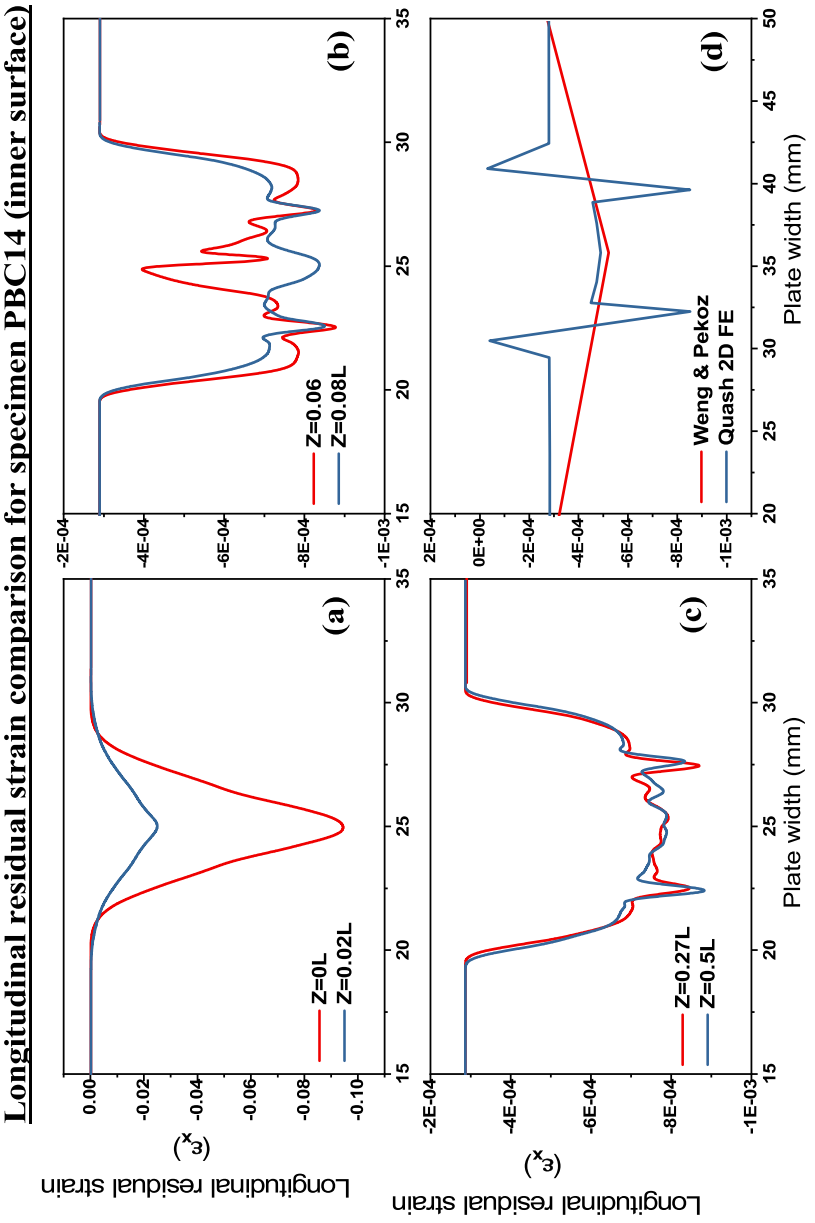


**Fig. 11.** Longitudinal residual strain comparison for specimen PBC14 (inner surface): (a) 3D-FE (0L and 0.02L), (b) 3D-FE (0.06L and 0.08L), (c) 3D-FE (0.27L and 0.5L), and (d) 2D-FE, Experiment.


https://doi.org/10.1016/j.heliyon.2018.e00937

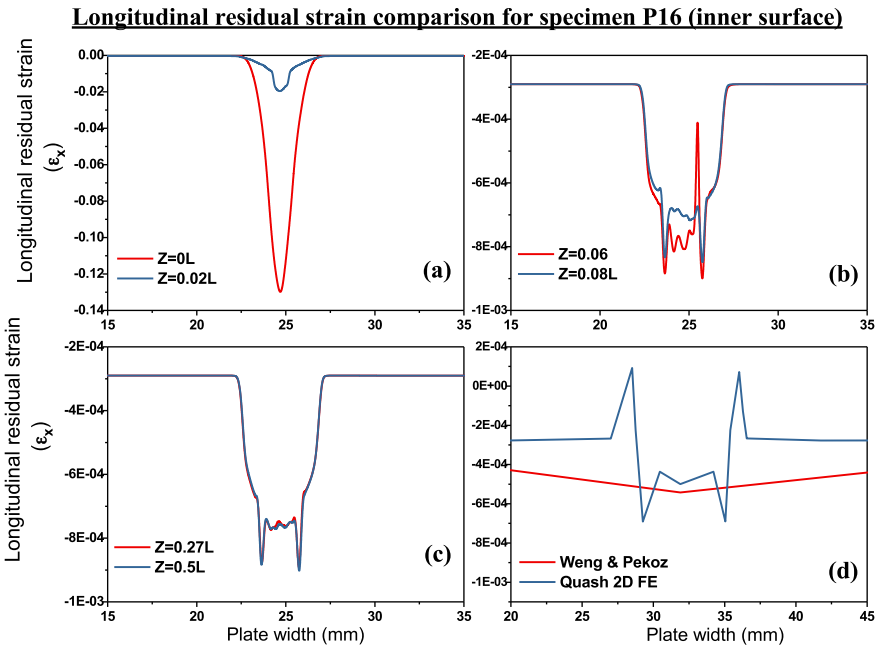


**Fig. 12.** Longitudinal residual strain comparison for specimen P16 (inner surface): (a) 3D-FE (0L and 0.02L), (b) 3D-FE (0.06L and 0.08L), (c) 3D-FE (0.27L and 0.5L), and (d) 2D-FE, Experiment.

### *3.3.2. Peak longitudinal residual strain comparison*

As mentioned in Section 2.1, this study was performed for a single bend to investigate the longitudinal residual strain. Hence, the results presented in this section is for a single corner perimeter of PBC14 and P16 sections. Longitudinal residual strain due to coiling-uncoiling process where determined from Eqs. (6), (7), (8), (9), (10), (11), (12), (13), and (14). These strain values added to results obtained from FE simulation for comparison purposes.

Figs. 9, 10, 11, and 12 show the comparisons between numerical results obtained in this study and the results presented by Weng and Quach et al. [5,7]. Figs. 9, 10, 11, and 12 present six different transverse lines. Those lines represent three different zones where the longitudinal residual strains have a significant change.

- Outer surface

In Fig. 9 (at the edge zone), longitudinal strains approach its highest at z = 0L and decline significantly at z = 0.02L. For Fig. 9b and c, no significant differences in the peak longitudinal strains. However, Fig. 9b appears to have more than one peak longitudinal strain at z = 0.06L. Fig. 9b and c show a close agreement with the results presented in Fig. 9d. But, Fig. 9a differentiates considerably from the experimental and 2D-FE results.

Similarly in Fig. 10, at the edge zone, the longitudinal residual strains approach its peak and decrease gradually till it gets closer to the experimental and 2D-FE results at the mid-plate zone.


https://doi.org/10.1016/j.heliyon.2018.e00937

- Inner surface

In Figs. 11 and 12, the longitudinal strains approach its highest at z = 0L and decline notably at z = 0.02L. For Graphs (b) and (c) in Figs. 11 and 12, no significant differences in the peak longitudinal strains. However, Graph (b) appears to have more than one peak longitudinal strain. Figs. 11b, c, 12b, and c show a close agreement with the results presented in Figs. 11d and 12d. Nevertheless, Figs. 11a and 12a differentiate considerably from the experimental and 2D-FE results.

## 3.4. Discussion

As explained in Section 3.2, high strains value occurred due to the lack of transverse restraint (free edge). This lack leads to a "softening" phenomenon where the plate edge tends to bend toward the normal direction when it was under a high transverse bending. This causes a significant difference in the longitudinal strain at the plate edge. So Graph (a) in Figs. 9, 10, 11, and 12 showed longitudinal strain at the highest in contrast with those in Graphs (b) & (c) in Figs. 9, 10, 11, and 12 where these strains decline away from the plate edge for the outer surface longitudinal strain. Hence, it is noticed that the longitudinal residual strain is not linear along the corner length. Experimental measurements may not be able to determine the longitudinal strain unless immediate measurement after fabrication process is done. 2D-FE showed a limitation in presenting results where it is unable to predict the changes along the corner length.

## 4. Conclusion

Cold work manufacturing processes normally produce cold formed steel sections. The amount of cold work to form the sections may induce residual stresses in the section, especially in the area of bending. These residual stresses play an important role on the section behavior and load-bearing capacity. In addition, longitudinal residual strain plays a significant role in formed section's load-bearing capacity. It raises during forming process, which is considered as one of the most important indicators that can be used to determine the geometric behavior of the formed section and in relation to the occurrence of defects such as local buckling [3]. A 3D finite element simulation in ABAQUS was employed to simulate this forming process. The study concluded that the longitudinal residual strain at the section corner edge was higher than those at the rest of the corner region. These strains at the edge were higher than the yield strain ($\boldsymbol{\varepsilon_y}$) of the formed section which occurred due to the lack of transverse restraint. This made the plate edge tended to bend toward the normal direction when it was under a high transverse bending. This causes a significant difference in the longitudinal strain at the plate edge.


https://doi.org/10.1016/j.heliyon.2018.e00937

## Declarations

### Author contribution statement

Ayad Mutafi: Analyzed and interpreted the data; Wrote the paper.

Noorfaizal Yidris: Conceived and designed the analysis; Analyzed and interpreted the data; Contributed analysis tools or data.

Mohamad R. Ishak, Rizal Zahari: Contributed analysis tools or data.

### Funding statement

This work was supported by Universiti Putra Malaysia and Ministry of Higher Education - Yemen.

### Competing interest statement

The authors declare no conflict of interest.

### Additional information

No additional information is available for this paper.

### Acknowledgements

This research is supported by the Yemen Ministry of Higher Education and the Fundamental Research Grant Scheme (FRGS) (Project Code: 03-02-13-1300FR) from Ministry of Higher Education, Malaysia.

## References

[1] J. Loughlan, N. Yidris, P.R. Cunningham, The effects of local buckling and material yielding on the axial stiffness and failure of uniformly compressed I-section and box-section struts, Thin Walled Struct. 49 (2) (2011) 264−279.

[2] W.M. Quach, J.G. Teng, K.F. Chung, Effect of the manufacturing process on the behaviour of press-braked thin-walled steel columns, Eng. Struct. 32 (11) (2010) 3501−3515.

[3] M.S. Tehrani, et al., Localised edge buckling in cold roll-forming of symmetric channel section, Thin Walled Struct. 44 (2) (2006) 184−196.

[4] M. Farzin, M. Salmani Tehrani, E. Shameli, Determination of buckling limit of strain in cold roll forming by the finite element analysis, J. Mater. Process. Technol. 125 (126) (2002) 626−632.


https://doi.org/10.1016/j.heliyon.2018.e00937

[5] C.C. Weng, P.T., Residual stresses in cold-formed steel members, J. Struct. Eng. 116 (6) (1990) 1611−1625.

[6] W.M. Quach, J.G. Teng, K.F. Chung, Residual stresses in steel sheets due to coiling and uncoiling: a closed-form analytical solution, Eng. Struct. 26 (9) (2004) 1249−1259.

[7] W.M. Quach, J.G. Teng, K.F. Chung, Finite element predictions of residual stresses in press-braked thin-walled steel sections, Eng. Struct. 28 (11) (2006) 1609−1619.

[8] H. Amouzegar, B.W. Schafer, M. Tootkaboni, An incremental numerical method for calculation of residual stresses and strains in cold-formed steel members, Thin Walled Struct. 106 (2016) 61−74.

[9] E.J. Gerbo, et al., Full-field measurement of residual strains in cold bent steel plates, J. Constr. Steel Res. 127 (2016) 187−203.

[10] M. Abambres, W.-M. Quach, Residual stresses in steel members: a review of available analytical expressions, Int. J. Struct. Integr. 7 (1) (2016) 70−94.

[11] ABAQUS 6.13-4, Dassault Systèmes Simulia Corp., Providence, RI, 2013.

[12] R.J. Kervick, S. Springborn, Cold Bending and Forming Tube and Other Sections, American Society of Tool and Manufacturing Enigneers Dearborn, MI, 1966.

[13] N.H. Cook, Manufacturing Analysis, Addison-Wesley Co., Reading, MA, 1966.

[14] W. Johnson, P.B. Mellor, Engineering Plasticity, Van Nostrand Reinhold, New York, NY, 1980.


https://doi.org/10.1016/j.heliyon.2018.e00937